



Nonlinear Mechanical FE Analysis of Thin-Plate Complex Structures Using the Shell-Solid Mixed Method

メタデータ	言語: eng 出版者: 公開日: 2021-06-17 キーワード (Ja): キーワード (En): 作成者: Ikushima, Kazuki メールアドレス: 所属:
URL	http://hdl.handle.net/10466/00017420

OMAE2020-19174

**NONLINEAR MECHANICAL FE ANALYSIS OF THIN-PLATE COMPLEX STRUCTURES
USING THE SHELL-SOLID MIXED METHOD**

Kazuki Ikushima
Osaka Prefecture University
Sakai, Osaka, Japan

ABSTRACT

In the construction of ships and ocean structures, thin steel plates are welded in order to join parts. Due to the welding, deformations and residual stresses may occur. These deformations and residual stresses can cause problems in the assembly process. Therefore, the prediction of welding deformations and residual stresses is necessary in advance of production. Welding deformations and residual stresses can be predicted using thermal elastic plastic (TEP) finite element analysis (FEA). However, solid elements are used in the conventional analysis method of TEP-FEA. The modeling of the thin-plate structures using solid elements is very complicated and difficult. In addition, the number of elements increases when using solid elements compared to shell elements. This leads to an increase in the required computing resources. Therefore, an efficient modeling method is necessary for thin-plate structures.

In the present research, in order to realize an efficient welding mechanics analysis method for thin-plate structures, the authors proposed an efficient FEA method for the welding mechanics problem for thin-plate complex structures using the proposed shell-solid mixed analysis method. For the shell-solid mixed analysis method, the multipoint constraint (MPC) technique was used in the finite element analysis to connect shell elements and solid elements. In order to compare the analysis accuracy with the conventional analysis, which uses solid elements, the proposed shell-solid mixed analysis method was applied to the fundamental welding mechanics problem of thin-plate structures. The results revealed that the proposed method has approximately the same analysis accuracy as the conventional method. These results indicated that the proposed method can effectively analyze the welding deformations and residual stresses in thin-plate complex structures.

INTRODUCTION

Ship structures are constructed by joining several thin plates and stiffeners by welding. Therefore, it is important to

investigate welding deformations and residual stresses in advance of fabrication. In order to predict welding deformations and residual stresses, TEP analysis based on finite element method (FEM) is usually used [1-3]. In TEP analysis, in order to predict welding deformations and residual stresses, consecutive analysis of transient nonlinear mechanical behavior due to heating is performed. Thus, the target of the analysis is divided into solid elements. This leads to difficulty in both modeling and the analysis scale.

On the other hand, ship structures are constructed of thin plates. Therefore, structural analysis of ship hulls is usually conducted using shell elements [4-6]. By using shell elements, the analysis model of the entire structure is easily extracted from the CAD data. Therefore, the difficulty in the analysis scale and modeling can be assumed to be removed by efficiently using both shell and solid elements, as compared to the case in which only solid elements are used for modeling.

Some examples are reported for the shell-solid mixed analysis. For example, 3D fracture mechanics analysis of a surface crack is conducted by FE software using rigid body elements [7]. Moreover, hot-spot stress is predicted using pseudo shell elements on the interface between solid and shell elements [8], and multi-scale analysis is conducted using the mesh superposition technique [9]. However, to the authors' knowledge, there is no example in which shell and solid elements are mixed in TEP analysis.

As such, in the present research, in order to construct an efficient welding TEP analysis model in the thin-plate complex structure, the authors propose a TEP analysis method that mixes shell elements and solid elements (shell-solid mixed analysis) by adopting the multipoint constraint (MPC) technique [10]. The proposed method is applied to the analysis of the fundamental welded joint and its characteristics are discussed. In addition, in order to demonstrate the applicability to the analysis of large complex thin-plate structures, the proposed method is applied to the analysis of welding of a cross joint in

the experimental mockup of the lower stool part in a bulk carrier.

SHELL-SOLID MIXED ANALYSIS METHOD

In the present research, in order to achieve an efficient modeling in welding mechanical analysis of thin-plate complex structures, the shell-solid mixed analysis method shown in Fig. 1 is proposed. In this concept, solid elements are used in the region in which the nonlinear elastic plastic analysis is required, and the other region is modeled by shell elements. Solid elements and shell elements are connected at their interface (shell-solid interface). By using this concept, the region that requires high-computing-load solid elements is reduced, and an efficient analysis can be expected.

In order to conduct a welding mechanics analysis, the temperature change due to the heat input is first predicted by heat conduction analysis. Then, according to the obtained temperature distribution, deformations and stresses are predicted by TEP analysis. By consecutively conducting this weak-coupled analysis from the start of welding to the complete cooling, the deformations and residual stresses after the welding are predicted. In this section, the shell-solid mixed analysis method used in the present research is described for each heat conduction analysis and thermal elastic plastic analysis.

Heat conduction analysis

In the heat conduction analysis, shell and solid elements are formulated based on the generic 2-D heat conduction element [11] and the generic 3-D heat conduction element [12],

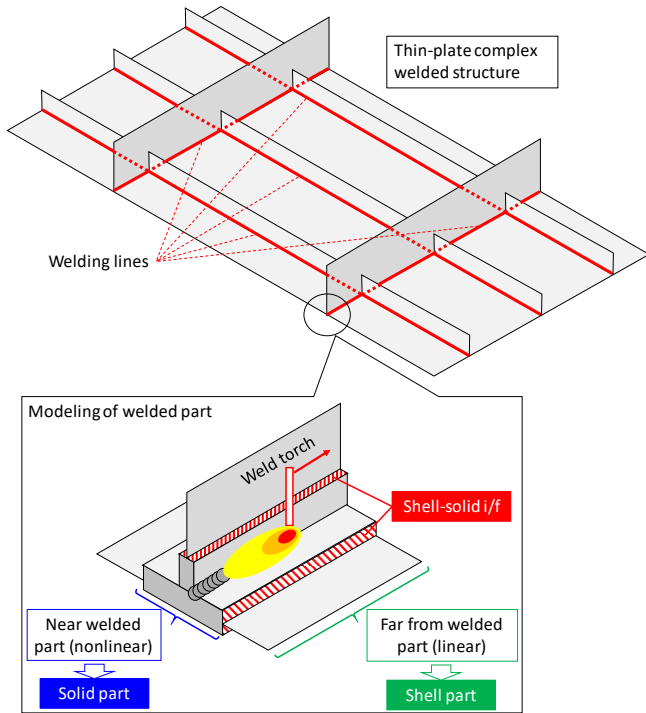


Figure 1. Concept of welding mechanics analysis based on shell-solid coupling.

respectively.

Connections between shell and solid elements are defined based on the method in which the degrees of freedom (DOFs) are erased [13]. As shown in Fig. 2, the MPC condition is configured such that the temperature of the nodes that are only connected to solid elements at the shell-solid interface is equal to that of shell elements. In other words, the relation between the nodal temperatures of shell and solid elements is defined by the following equation as the constraint condition:

$$T_{solid} = T_{shell} \quad (1)$$

where T_{solid} and T_{shell} are the nodal temperatures of solid and shell elements, respectively. In order to consider the constraint condition of Eq. (1), the DOFs belonging to the nodes connected only to a solid element at the shell-solid interface are erased. In the following, the nodes of shell elements are defined collectively as the master node, and the nodes of solid elements are defined as slave node. In order to adopt the relation described by Eq. (1), this relation is expressed in the following matrix form:

$$\mathbf{B}^h \mathbf{u}^h = \{0\} \quad (2)$$

where \mathbf{B}^h and \mathbf{u}^h are the matrices of the constraint condition and the DOF (temperature) vector, respectively. In the constraint condition of Eq. (2), dividing the DOF vector \mathbf{u}^h by the vector of the independent component (master node) \mathbf{u}_m^h and that of the dependent component (slave node) \mathbf{u}_s^h , yields:

$$[\mathbf{B}_s^h \quad \mathbf{B}_m^h] \begin{Bmatrix} \mathbf{u}_s^h \\ \mathbf{u}_m^h \end{Bmatrix} = \{0\} \quad (3)$$

where \mathbf{B}_s^h and \mathbf{B}_m^h are the constraint condition matrices for the slave DOFs and the master DOFs, respectively. Using Eq. (3), the entire DOF vector is expressed as:

$$\mathbf{u}^h = \mathbf{T}^h \mathbf{u}_m^h \quad (4)$$

$$\mathbf{T}^h = \begin{bmatrix} -\mathbf{B}_s^h{}^{-1} \mathbf{B}_m^h \\ \mathbf{I} \end{bmatrix} \quad (5)$$

In the above equation, \mathbf{I} is a unit matrix. The simultaneous

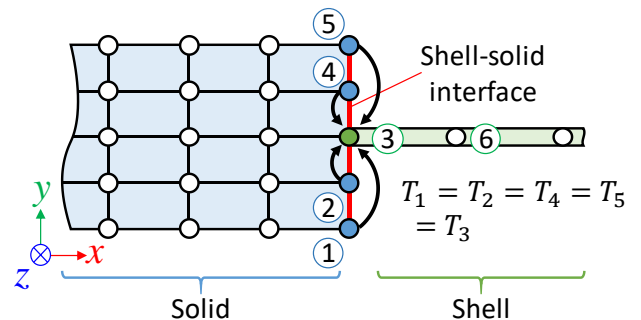


Figure 2. Schematic diagram of shell-solid coupling in heat conduction analysis.

equations obtained by discretizing the unsteady heat conduction problem using the finite element formulation are defined by Eq. (6). Substituting Eq. (4) into Eq. (6) and multiplying by \mathbf{T}^h yields Eq. (7), as follows:

$$\mathbf{K}^h \mathbf{u}^h = \mathbf{q} \quad (6)$$

$$\mathbf{T}^{hT} \mathbf{K}^h \mathbf{T}^h \mathbf{u}_m^h = \mathbf{T}^{hT} \mathbf{q} \quad (7)$$

where \mathbf{K}^h and \mathbf{q} are the coefficient matrix and the heat vector, respectively. As shown in Eq. (7), the DOFs for the slave nodes are erased.

As an example, assuming that the nodes are indexed in the order shown in Fig. 2, the constraint condition matrix \mathbf{T}^h , the vector for the slave DOF, \mathbf{u}_s^h , and the vector for the master DOF, \mathbf{u}_m^h , are defined as follows:

$$\mathbf{B}^h = \begin{bmatrix} 1 & 0 & -1 & 0 & 0 & 0 \\ 0 & 1 & -1 & 0 & 0 & 0 \\ 0 & 0 & -1 & 1 & 0 & 0 \\ 0 & 0 & -1 & 0 & 1 & 0 \end{bmatrix}, \quad (8)$$

$$\mathbf{T}^h = \begin{bmatrix} 1 & 0 \\ 1 & 0 \\ 1 & 0 \\ 1 & 0 \\ 1 & 0 \\ 0 & 1 \end{bmatrix}, \quad \mathbf{u}_s^h = \begin{Bmatrix} T_1 \\ T_2 \\ T_4 \\ T_5 \end{Bmatrix}, \quad \mathbf{u}_m^h = \begin{Bmatrix} T_3 \\ T_6 \end{Bmatrix}$$

Using Eq. (8), Eq. (7) is then rewritten as:

$$[\mathbf{T}^h]^T [\mathbf{K}^h] [\mathbf{T}^h] \begin{Bmatrix} T_3 \\ T_6 \end{Bmatrix} = [\mathbf{T}^h]^T \{\mathbf{q}\} \quad (9)$$

Based on the above equation, the slave DOF on the shell-solid interface is confirmed to have been erased.

Thermal elastic plastic analysis

An MITC4 element [14] is used for the formulation of the shell element. The MITC4 element is widely used in FE software and is a degenerated shell element [15] that degenerates a solid element to the neutral plane. In the MITC4 element, the accuracy for the bending deformation is improved by modifying the evaluation of the strain component for shear deformation. The shell element is assumed to be an elastic body so as not to consider plastic deformation for the computational efficiency.

In addition, the generic solid element has only the DOF of displacement, whereas the shell element has a rotational DOF. In order to unify the number of DOFs for the entire node, a solid element with a rotational DOF [16] is used in the present research. In the formulation of this element, mid-point nodes of a hexahedral element with 20 nodes are degenerated to give the rotational DOF at each vertex of a hexahedral element with eight nodes. The analysis accuracy of this element is approximately the same as that of a hexahedral element with 20 nodes [16].

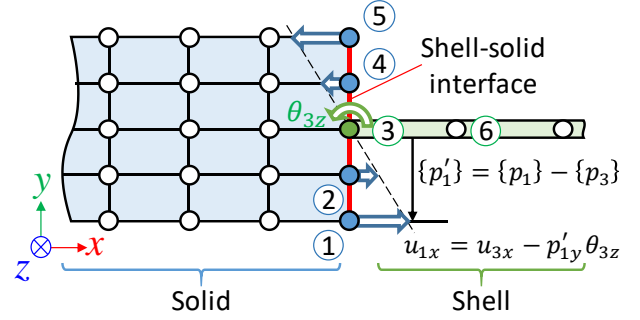


Figure 3. Schematic diagram of shell-solid coupling in mechanical analysis.

In the same way as shown in the previous section, the DOF at the shell-solid interface is erased in TEP analysis using MPC. However, the node in TEP analysis has six DOFs (three translation + three rotation), which must be considered. In addition, as shown in Fig. 3, the DOF of the slave node must satisfy the following relation because the shape of the cross section of the shell element at the shell-solid interface must be maintained.

$$\mathbf{u}_s^m = \mathbf{B}_m^m \mathbf{u}_m^m \quad (10)$$

$$\mathbf{u}_s^m = \begin{Bmatrix} v_{sx} \\ v_{sy} \\ v_{sz} \\ \theta_{sx} \\ \theta_{sy} \\ \theta_{sz} \end{Bmatrix}, \quad \mathbf{u}_m^m = \begin{Bmatrix} v_{mx} \\ v_{my} \\ v_{mz} \\ \theta_{mx} \\ \theta_{my} \\ \theta_{mz} \end{Bmatrix} \quad (11)$$

$$\mathbf{B}_m^m = \begin{bmatrix} 1 & 0 & 0 & 0 & p'_{sz} & -p'_{sy} \\ 0 & 1 & 0 & -p'_{sz} & 0 & p'_{sx} \\ 0 & 0 & 1 & p'_{sy} & -p'_{sx} & 0 \\ 0 & 0 & 0 & 1 & 0 & 0 \\ 0 & 0 & 0 & 0 & 1 & 0 \\ 0 & 0 & 0 & 0 & 0 & 1 \end{bmatrix} \quad (12)$$

where \mathbf{u}_s^m and \mathbf{u}_m^m are the DOF vectors for the slave and master nodes, respectively, and v_s , θ_s , v_m , and θ_m are the translational and rotational DOFs for the slave and master nodes, respectively. The suffixes x, y, and z indicate the direction of the DOF. Here, p'_s is the relative position of the slave node from the master node. By using Eq. (10) as the MPC condition, it is possible to configure a constraint condition that maintains the shape of the cross section of the shell element because Eq. (10) considers the rigid body rotation due to the rotational DOF in the master node. In the same way as in the previous section, considering the constraint condition of Eq. (10) on the simultaneous equations (Eq. (13)) obtained by discretizing the TEP problem using the FEM, yields Eq. (14):

$$\mathbf{K}^m \Delta \mathbf{u}^m = \Delta \mathbf{F} \quad (13)$$

$$\mathbf{T}^{mT} \mathbf{K}^m \mathbf{T}^m \Delta \mathbf{u}_m^m = \mathbf{T}^{mT} \Delta \mathbf{F} \quad (14)$$

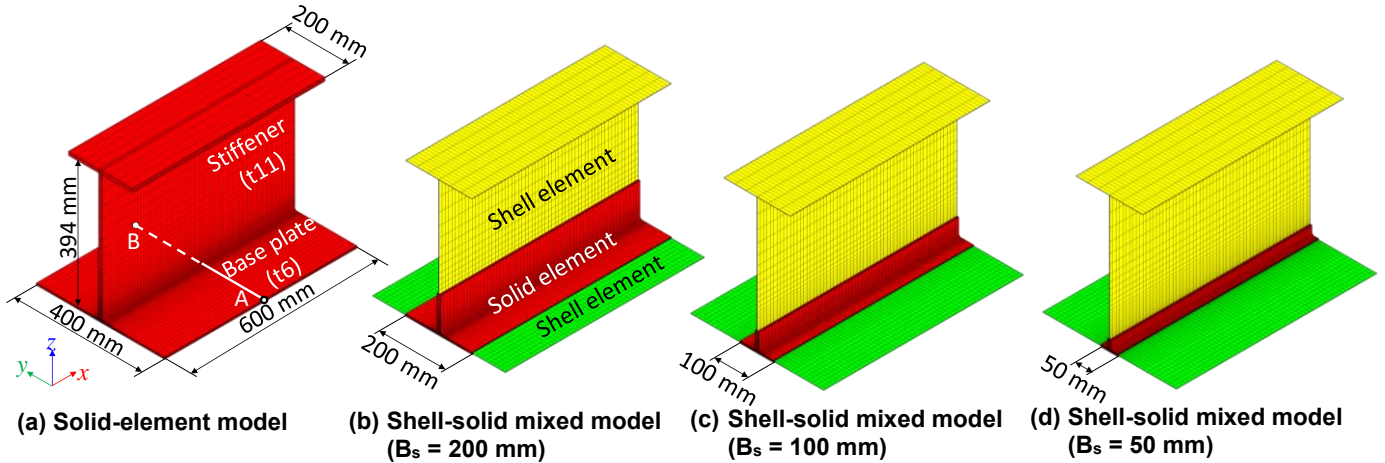


Figure 4. Analysis model of stiffened plate.

where K^m , Δu^m , ΔF , and Δu_m^m are the entire stiffness matrix, the displacement increment vector, the load increment vector, and the displacement increment vector for the master node, respectively. The constraint matrix T^m is defined as follows:

$$T^m = \begin{bmatrix} B_{m1}^m \\ B_{m2}^m \\ \vdots \\ B_{mi}^m \\ \vdots \\ I \end{bmatrix} \quad (15)$$

where submatrix B_{mi}^m is the constraint condition for each slave node i determined by Eq. (12). Using the above expression, shell and solid elements are connected by erasing the DOF for the solid element at the shell-solid interface.

The analysis procedure described above is implemented on the in-house analysis program for the welding mechanics problem based on the Idealized Explicit FEM [17]. This program implements a parallel computation using a graphics processing unit (GPU). In the implementation of the proposed method, the master node is defined as the node at the shell-solid interface belonging to the shell element. The slave node is defined as the node at the shell-solid interface belonging only to the solid element. The slave node is automatically selected by the program as the node located in the normal direction of the shell element from the master node and located within the thickness of the shell element.

VALIDATION OF THE PROPOSED METHOD

Analysis model and condition

In order to discuss the capability of the proposed method, the proposed method and the ordinary TEP analysis method using solid elements [17] are applied to the analysis of the fundamental weld joint shown in Fig. 4. As shown in the figure,

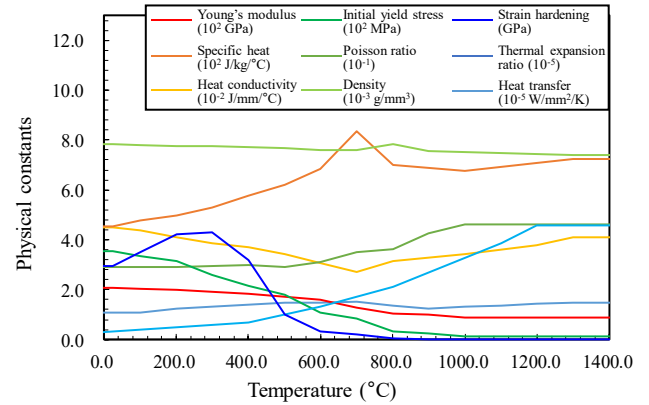


Figure 5. Temperature-dependent material properties of SM490A.

the analysis model has a base plate with a length of 600 mm, a width of 400 mm, and a thickness of 6 mm, and a stiffener with a height of 394 mm, a thickness of 11 mm, and a flange width of 200 mm. Both sides of the joint between the base plate and stiffener were welded. The material of the base plate and stiffener is assumed to be SM490A. The temperature-dependent material properties of SM490A are shown in Fig. 5 [18]. The welding condition was assumed as follows: current = 330 A, voltage = 32 V, welding speed = 10 mm/s, and heat efficiency = 0.8. The room temperature was assumed to be 20°C.

Accuracy of the proposed method

It is desirable that the welded part be modeled with solid elements because the welded part exhibits complex nonlinear mechanical behavior. The other part exhibits linear elastic mechanical behavior, which can be modeled by shell elements. In this section, the effect of the dimension of the region in which solid elements are used on the analysis accuracy is investigated.

The analysis models used in this investigation are shown in Figs. 4(b) through 4(d), where the widths of the region in which solid elements are used (B_s) was varied as 200 mm, 100 mm, and 50 mm, respectively. The other region is modeled by shell

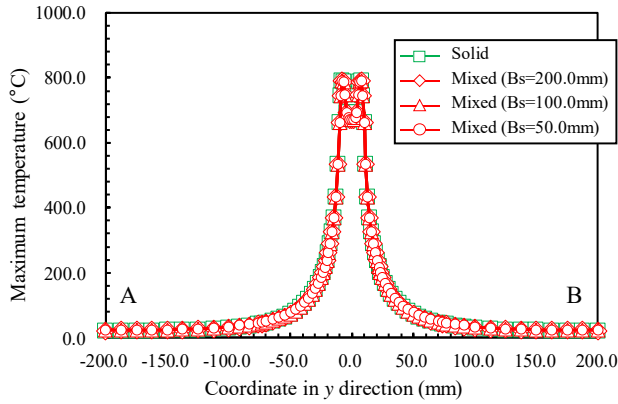


Figure 6. Maximum temperature distribution along line A-B.

elements. Figure 4(a) shows the reference model, which is meshed with solid elements (hexahedral elements with eight nodes). As a result of mesh division, the number of elements in each model shown in Figs. 4(a) through 4(d) are 49,200, 41,160 (39,120 solid, 2,040 shell), 34,080 (30,600 solid, 2,480 shell), and 25,920 (21,000 solid, 4,920 shell), respectively.

Figure 6 shows the maximum temperature distribution after

welding along line A-B, shown in Fig. 4(a), located at the center of thickness on the transverse cross section at the center of the welding line. In the figure, the \diamond , \triangle , and \circ symbols with the solid red lines indicate the analysis results for the model with $B_s = 200$ mm, 100 mm, and 50 mm, respectively. The \square symbols with the solid green line indicate the analysis results for the reference solid model. As shown in Fig. 6, the welded part and its vicinity reached the mechanical melting point of the material in all models. In addition, in the shell-solid mixed model, a continuous temperature distribution was obtained, regardless of the width of the solid region, and the temperature distribution in the shell-solid model has almost no difference as compared to the reference solid model.

Figure 7 shows the distribution of equivalent stress after 35 s from the start of welding. In the figure, (a) shows the results obtained for the reference solid model, and (b) through (d) show the results for the models with $B_s = 200$ mm, 100 mm, and 50 mm, respectively. As shown in Fig. 7, the vicinity of the weld torch has a small equivalent stress because the yield stress decreases due to the high temperature. After the weld torch passes and the temperature decreases by cooling, the equivalent stress increases because the yield stress recovers to that at room

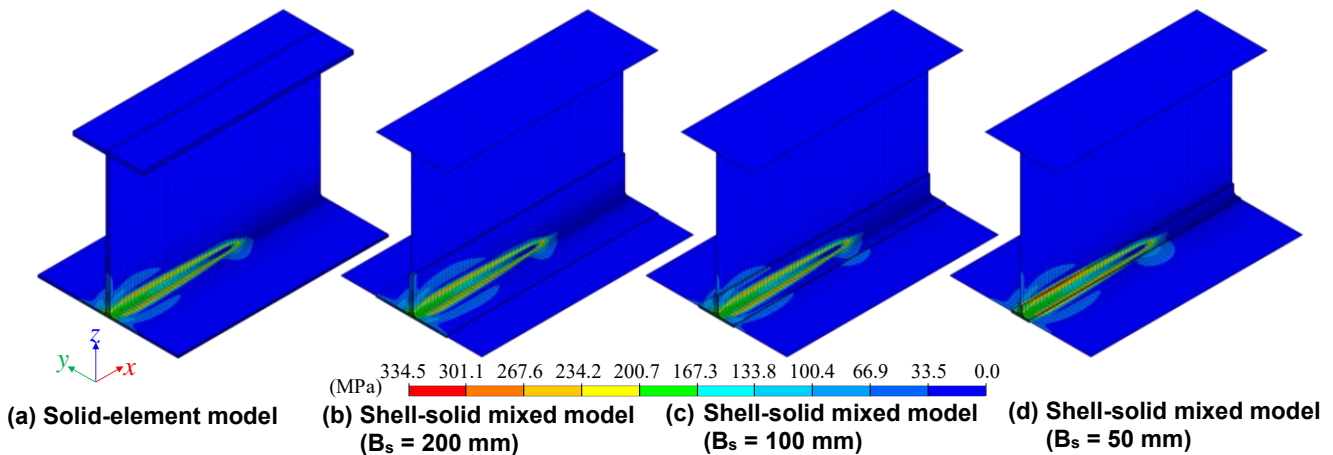


Figure 7. Distribution of equivalent stress ($\bar{\sigma}$) at 35 s from the start of welding.

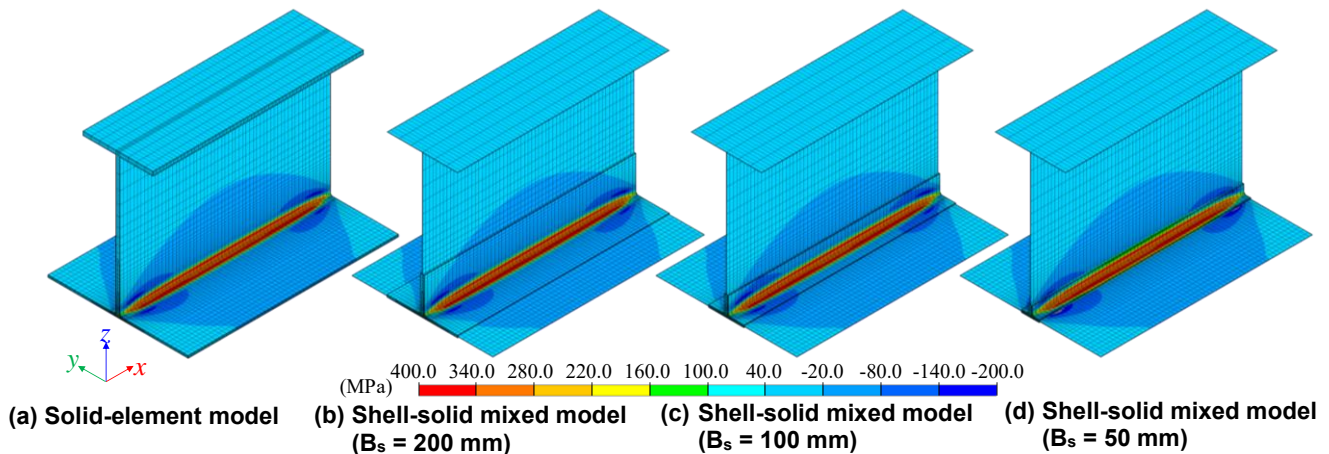


Figure 8. Distribution of residual stress in the x direction (σ_{xx}).

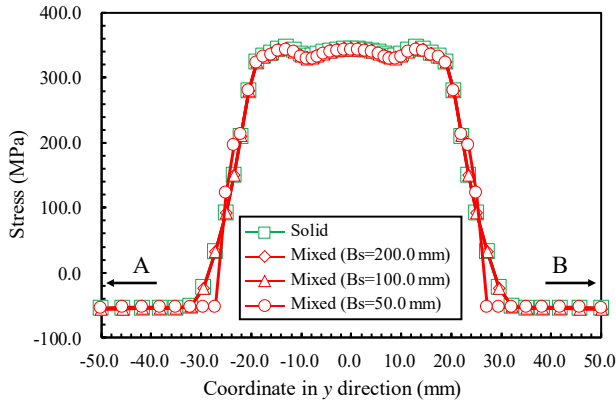


Figure 9. Distribution of residual stress in the x direction (σ_{xx}) along line A-B near the welded part.

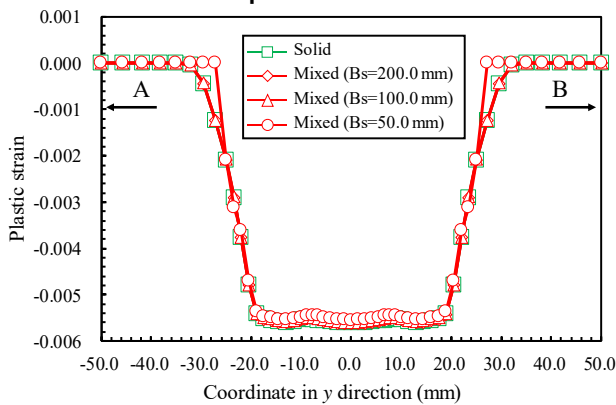


Figure 10. Distribution of plastic strain in the x direction (ϵ_{xx}^p) after welding along line A-B near the welded part.

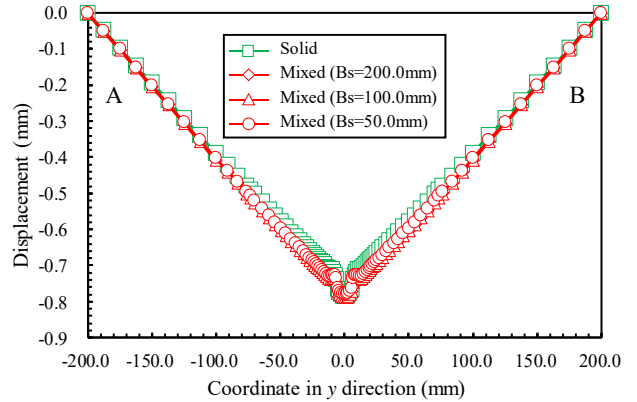


Figure 11. Distribution of angular distortion.

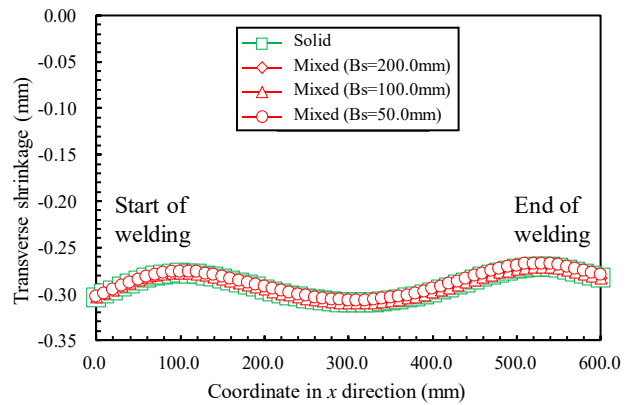


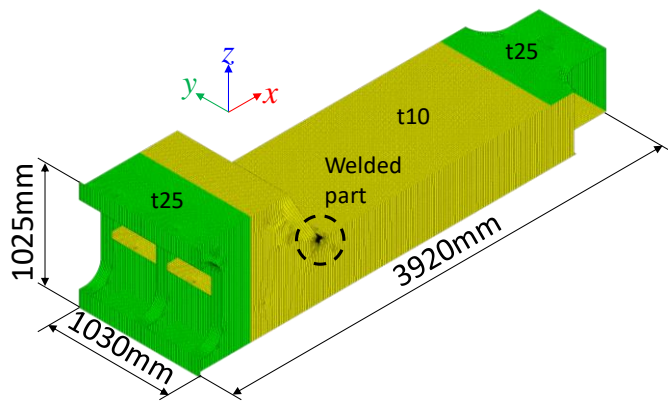
Figure 12. Distribution of transverse shrinkage.

temperature (20°C). In addition, the equivalent stress distribution approximately agrees among all models, but the stress distribution in the model with $B_s = 100$ mm (Fig. 7(c)) is different from the stress distributions in the other models. This is because the equivalent stress of the shell element is an element-averaged value, which is almost the same as the stress at the element center, whereas that of the solid element shows the stress on the surface of the plate. Regarding the model having the smallest $B_s (= 50$ mm) (Fig. 7(d)), the equivalent stress on the shell-solid interface is larger than in the other models. The MPC condition can be assumed to restrict the deformation of the shell-solid interface to maintain the shape of the cross section of the shell element. Therefore, the thermal expansion in the thickness direction is constrained, and the stress increases.

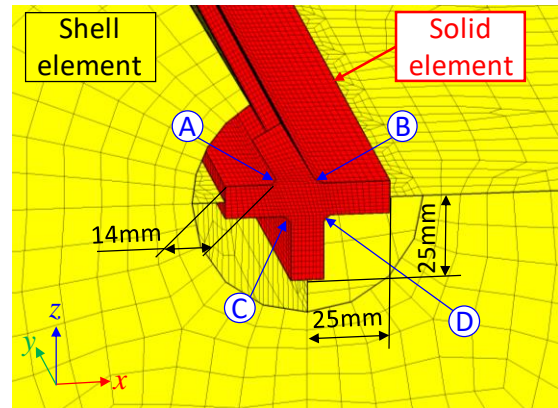
The residual stress distribution in the x direction (σ_{xx}) after welding is shown in Fig. 8. Figure 9 shows the distribution of residual stress in the x direction (σ_{xx}) near the welded part along line A-B. These figures indicate that the typical residual stress due to welding is obtained. The tensile stress occurs in the welded part and its vicinity, and other regions have a compressive stress that balances the tensile stress. The residual stress distribution also has a continuous distribution on the

shell-solid interface, and the tendency of the stress distribution in the entire model agrees among all models. However, the stress distribution for the model having the smallest $B_s (= 50$ mm) (Fig. 4(d)) has a slight difference in the vicinity of the welded part. The reason for this can be assumed to be that the difference occurs because the nonlinear elastic plastic deformation is considered only in solid elements, whereas shell elements assume an elastic body. Figure 10 shows the distribution of plastic strain in the x direction (ϵ_{xx}^p) near the welded part along line A-B. Based on Fig. 10, plastic strain does not occur outside the solid region ($y = -25$ mm to 25 mm) for the $B_s = 50$ mm model because an elastic body is assumed for shell elements. In the other models, plastic strain occurs in the region outside $y = -25$ mm to 25 mm. This difference in plastic strain can be assumed to cause the difference in stress distribution.

In order to discuss the welding deformation, the distributions of angular distortion and transverse shrinkage are shown in Figs. 11 and 12, respectively. The angular distortion is defined as the difference of the position in the z direction from the line A-B in the deformed shape after welding. The transverse shrinkage is defined as the difference in displacement in the y direction between the right and left edges of the base plate. From Fig. 11, regarding the angular distortion,



(a) Overall view



(b) Close-up view of the welded part

Figure 13. Analysis model of the test body of the lower stool in a bulk carrier.

a V-shaped deformation, in which the welded part sinks, is obtained. There is almost no difference among the shell-solid mixed models and the reference solid model with regard to the angular distortion, and approximately the same results are obtained. Regarding the transverse shrinkage shown in Fig. 12, a shrinkage of approximately 0.3 mm occurs for the entire length, and the difference among the shell-solid mixed models and the reference model is very small.

As shown in this section, the proposed method can be assumed to have approximately the same analysis accuracy as the solid element model with regard to the welding deformation and residual stress, unless plastic deformation occurs at the shell-solid interface.

APPLICATION TO COMPLEX STRUCTURES

Analysis model and conditions

In order to demonstrate the applicability of the proposed method to a realistic structure, the proposed method is applied to the analysis referencing the cross weld joint in the strength test body of the lower stool in a bulk carrier [19]. The weld toe in a cross joint, such as the base part of the lower stool, is known to be a location at which fatigue fracturing frequently occurs [20]. Therefore, this part is assumed to have a certain effect of residual stress due to the welding assembly.

Figure 13(a) shows an overall view of the analysis model. The analysis model is 3,920 mm in length, 1,030 mm in width, and 1,025 mm in height. The analysis model is meshed with 15 mm square shell elements and solid elements of 5 mm in length. As a result of mesh divisions, the numbers of nodes, DOFs, shell elements, and solid elements are 223,273, 1,339,632, 88,439, and 119,400, respectively. The material is assumed to be SM490A, as in the previous chapter. The number of weldings is four, and the welding passes are labeled A through D, as shown in Fig. 13(b). The passes are welded in the order of A, B, C, and D. The welding condition is assumed to be as follows: current = 180 A, voltage = 18 V, welding speed = 8 mm/s, and heat efficiency = 0.8. The welding is conducted in the y direction from negative to positive. As shown in Fig.

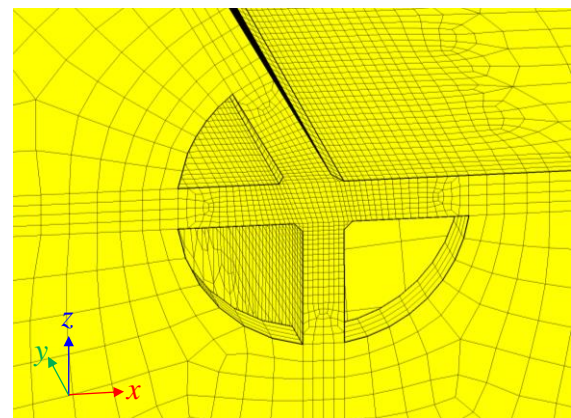


Figure 14. Mesh division of the reference solid model near the welded part.

13(b), solid elements are used in the welded part and its vicinity. Other regions, including the overall structure, are modeled by shell elements. For the constraint condition, only the rigid body motion mode is constrained.

For the comparison, the same analysis model is prepared with solid, linear, hexahedral elements. For example, the mesh division near the welded part is shown in Fig. 14. In the modeling with only hexahedral elements, mesh division considering the thickness direction is necessary, and very complicated work is required. In addition, as a result of mesh division, the analysis scale increases. In regions other than the welded part, the size of the elements is 15 mm square, and the number of elements in the thickness direction is four. The number of nodes, DOFs, and elements are 643,382, 1,930,146, and 533,104, respectively. The analysis scale increases in the analysis with solid elements because the number of nodes is almost tripled, as compared with that of the shell-solid mixed model.

The computer used in this analysis has an Intel Core i9 3.3-GHz processor as a CPU and an NVIDIA GeForce RTX 2080Ti processor as a GPU. As a result of heat conduction analysis, the number of temperature steps becomes 12,941. Thermal elastic plastic analysis is conducted for these temperature steps.

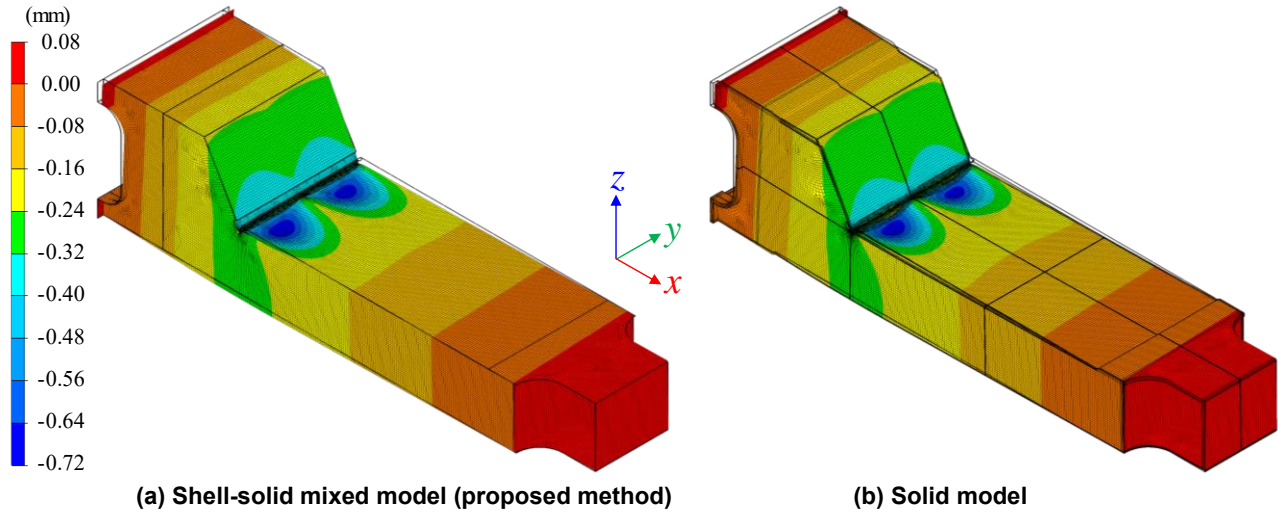


Figure 15. Distribution of displacement in the z direction with deformed shape after welding.

Analysis results

The deformed shape and distribution of the displacement in the z direction after the four welding passes are shown in Fig. 15. In the figure, (a) and (b) show the analysis results for the shell-solid mixed model and the solid model, respectively. The deformation is magnified by 150, and the shape before welding is also shown as outlines. As shown in Fig. 15, the transverse shrinkage after the final pass occurs on the top plate above the neutral surface, which causes the sinking deformation in the z direction for the entire structure. In the near part of the welding, the angular distortion due to the final pass leads to the hungry-horse-like deformation, in which the top plate deflects toward the inside. However, the welded part of this model is relatively small as compared to the entire structure, and the welding deformation is less than 1 mm. The tendency and amount of the welding deformation in both models are in good agreement.

The above results indicate that the proposed method can predict the welding deformation and residual stress in a complex structure with approximately the same accuracy as the existing method. The computing time for this analysis was approximately nine hours for the shell-solid model and 16 hours for the solid model. This means that efficient analysis can be achieved using solid elements in the welded part and its vicinity. In addition, preparing an analysis model with hexahedral elements is extremely difficult because automatic mesh generation is currently not established. Therefore, manual mesh division is required, which increases the labor cost. On the other hand, automatic mesh generation is available for tetrahedral elements, such as the Delaunay tetrahedralization [21]. However, in thin-plate large structures, such as ships, numerous tetrahedral elements may be required in order to obtain a good-quality mesh, which has a low aspect ratio. Using the proposed method, a detailed analysis can be achieved by locally embedding solid elements into the shell element model used in the structural analysis generated from a CAD model.

This indicates that the proposed method is effective for efficient and accurate analysis of complex structures. The MPC function and element formulations used in the present research have been implemented in commercial FE software [22]. Therefore, it is also possible to construct an analysis system based on the proposed method using commercial FE software, and efficient computation can be expected.

CONCLUSIONS

In the present research, in order to achieve an efficient welding mechanics analysis in complex thin-plate structures, a shell-solid mixed analysis method was proposed. In the proposed method, shell elements and solid elements are connected by erasing DOFs using the MPC. In the welding mechanics analysis, both heat conduction analysis and thermal elastic plastic analysis are conducted. Therefore, shell-solid mixed analysis was formulated for both analyses. The proposed method was applied to the analysis of the fundamental weld joint and the complex structure of the cross weld joint in the test body of the lower stool in a bulk carrier. The following results were obtained.

The proposed method was applied to the welding mechanics analysis of the fundamental weld joint. The influence of the dimension of the solid element region in the proposed method was investigated. The results reveal that the proposed method can analyze welding mechanical problems with approximately the same accuracy as the conventional method using solid elements, unless plastic strain occurs at the shell-solid boundary.

In order to demonstrate the applicability to complex large-scale structures, the proposed method was applied to the analysis of the cross weld joint in the strength test body of the lower stool in a bulk carrier. As a result, the proposed method was demonstrated to yield approximately the same results as the conventional method. The computational time of the

proposed method was approximately half of that of the conventional method using solid elements.

REFERENCES

- [1] Ueda, Y., Yamakawa, T., “Analysis of thermal elastic-plastic behavior of metals during welding by finite element method”, *Transactions of The Japan Welding Society*, Vol.42, No.6, pp.567-577, 1973.
- [2] Nishikawa, H., Serizawa, H., Murakawa, H., “Actual application of large-scaled FEM for analysis of mechanical problems in welding”, *Quarterly Journal of the Japan Welding Society*, Vol.24, No.2, pp.168-173, 2006.
- [3] Goldak, J., Mocarita, M., Aldea, V., Zhou, J., Downey, D., Dorling, D., “Predicting Burn-through When Welding on Pressurized Natural Gas Pipelines”, *Proceedings of 2000 ASME Pressure Vessels and Piping Conference*, pp.23-27, 2000.
- [4] Tatsumi, A., Fujikubo, M., “Ultimate Longitudinal Strength Analysis of Container Ships Considering Bottom Local Loads - Part 1: Nonlinear Finite Element Analysis -”, *Journal of the Japan Society of Naval Architects and Ocean Engineers*, Vol.24, pp.189-198, 2016.
- [5] Naruse, Y., Kawamura, Y., Okada, T., “A Study on Estimation Method of Ship Hull Girder Ultimate Strength under Biaxial Compression”, *Journal of the Japan Society of Naval Architects and Ocean Engineers*, Vol.23, pp.239-249, 2016.
- [6] Toh, K., Toshikawa, T., “A Study on the Hull Girder Ultimate Strength of Intact and Damaged Hull Structures”, *Journal of the Japan Society of Naval Architects and Ocean Engineers*, Vol.22, pp.137-150, 2015.
- [7] Tanaka, S., Okada, H., Okazawa, S., Xi, Y., Ohtsuki, Y., “Three-dimensional fracture mechanics analysis of surface crack in ship structure using shell-solid mixed analysis”, *Journal of the Japan Society of Naval Architects and Ocean Engineers*, Vol.13, pp.147-155, 2011.
- [8] Osawa, N., Hashimoto, K., Sawamura, J., Nakai, T., Suzuki, S., “Study on shell-solid coupling FE analysis for fatigue assessment of ship structure”, *Marine Structures*, Vol.20, pp.143-163, 2007.
- [9] Suzuki, K., Otsubo, H., Min, S., Shiraishi, T., “Multi scale analysis of ship structure using Overlaying mesh method”, *Transactions of JSCES*, Vol.1999, paper no.19990020, 1999.
- [10] Belytschko, T., Liu, W.K., Moran, B., “Nonlinear finite elements for continua and structures”, *Wiley*, 2000.
- [11] Yagawa, G., Miyazaki, N., “Analysis of thermal stress, creep and heat conduction by finite element method”, *Science-Sha*, 1985.
- [12] Touno, T., “Heat conduction and thermal stress”, *Baifukan*, 1972.
- [13] Goto, K., Hashimoto, G., Okuda, H., “Convergence of Parallel Iterative Linear Solver in Treatment of Multipoint Constraints With Implicit and Explicit Master-slave Elimination”, *Transaction of the Japan Society for Simulation Technology*, Vol.7, No.1, pp.1-9, 2015.
- [14] Dvorkin, E. N., Bathe, K. J., “A continuum mechanics based for-node shell element for general nonlinear analysis”, *Engineering Computations*, Vol.1 No.1, pp.77-88, 1984.
- [15] Ahmad, S., Irons, B. M., Zienkiewicz, O. C., “Analysis of thick and thin shell structures by curved finite elements”, *International Journal for Numerical Methods in Engineering*, Vol.2, pp.419-451, 1970.
- [16] Yunus, S. M., Pawlak, T. P., Cook, R. D., “Solid elements with rotational degrees of freedom: Part 1 -Hexahedron elements”, *International Journal for Numerical Methods in Engineering*, Vol.31, pp.573-592, 1991.
- [17] Ikushima, K., Shibahara, M., “Nonlinear computational welding mechanics for large structures”, *Journal of Offshore Mechanics and Arctic Engineering*, Vol.141, No.2, paper no.021603, 2019.
- [18] Japan Nuclear Energy Safety Organization, “Project of Integrity Assessment of Flawed Components with Structural Discontinuity (IAF) Material Properties Data Book at High Temperature for dissimilar metal welding in Reactor Pressure Vessel”, *JNES-RE-Report Series*, 2013.
- [19] Osawa, N., Yamamoto, N., Fukuoka, T., Sawamura, J., Nagai, H., Maeda, S., “Study on the Preciseness of Hot Spot Stress of Web-Stiffened Cruciform Welded Joints Derived by Shell Finite Element Analyses”, *Journal of the Japan Society of Naval Architects and Ocean Engineers*, Vol.14, pp.175-189, 2011.
- [20] Tanaka, Y., Ogawa, H., Yagi, K., Osawa, N., “Large-scale weld mock-up”, *Bulletin of The Japan Society of Naval Architects and Ocean Engineers*, Vol.65, pp.20-29, 2016.
- [21] Yamada, T., Kawai, H., “Mesh Generation in Finite Element Analysis”, *Journal of the Japan Society for Precision Engineering*, Vol.76, No.11, pp.1244-1247, 2011.
- [22] ANSYS Inc., “ANSYS Theory Reference Release 5.6”, 1994.